High-Alfa Aerodynamics with Separated Flow Modeled as a Single Nascent Vortex

High-Alfa Aerodynamics with Separated Flow Modeled as a Single Nascent Vortex

Antony Samuel B
MS Scholar
Dept.of Applied Mechanics, Indian Institute of Technology Madras, India 600036.
E-mail: antonysamuelb@gmail.com

Rinku Mukherjee
Assistant Professor
Dept.of Applied Mechanics, Indian Institute of Technology Madras, India 600036.
E-mail: rinku@iitm.ac.in

Abstract. A numerical iterative vortex lattice method is developed to study flow past wing(s) at high angles of attack where the separated flow is modelled using NY nascent vortex filaments. The wing itself is modelled using $NX \times NY$ bound vortex rings, where NX and NY are the number of sections along the chord and span of the wing respectively. The strength and position of the nascent vortex along the chord corresponding to the local effective angle of attack are evaluated from the residuals in viscous and potential flow, i.e. $(C_l)_{visc} - (C_l)_{pot}$ and $(C_m)_{visc} - (C_m)_{pot}$. Hence, the 2D airfoil viscous $C_l - \alpha$ and $C_m - \alpha$ is required as input (from experiment, numerical analysis or CFD). Aerodynamic characteristics and section distribution along span are predicted for 3D wings at a high angle of attack. Effect of initial conditions and existence of multiple solutions in the post-stall region is studied. Results are validated with experiment.

1. Introduction

The interest in extending linear methods to include post-stall regimes of flow has existed since Prandtl's Lifting Line Theory. A vortex-lattice method algorithm based on a novel decambering approach [1] uses an estimate of the reduction in camber at post-stall angles of attack to account for the change in C_l and C_m from the inviscid case.

Sarpakaya [2] in his review paper, discusses shedding of discrete vortices from the points of separation. He mentions that vortex methods are the weakest when used for simulating separated flows. Various methods, using both variable and fixed positions of the nascent vortex have been discussed while the strength of the circulation of the discrete shed vortex at each time step is found out from the velocity at a certain point, e.g. at the position of the nascent vortex.

Katz [3] places the separated vortex at the half way point of the distance covered in a given time step, by the panel LE in which the separation point lies. The separation point in this case is previously known. The magnitude of circulation of Nascent Vortex shed is calculated using velocities across the shear layer. Antonini et al [4] uses C_l value of the airfoil to find the point of separation and the separated nascent vortex is placed at a certain predetermined distance from the point of separation. Sarpakaya [5] estimates the velocity which is used for calculating the strength of the shed vortex by taking the average velocity of 4 previously shed vortices. The position of the nascent vortex is selected in such a way that the kutta condition is satisfied. Chorin [6] has set a different path, wherein nascent vortices are introduced throughout the surface. No-slip condition is applied at the boundary in order to find the strength and the core radius of the Nascent Vortices. The method has been used to predict the temporal loading on a cylinder.

Separated flow, especially post stall is an unsteady phenomenon. The motivation of the current work is to incorporate viscous effect into a 2D discrete vortex method and a 3D vortex lattice method, while also being able to predict the position of and strength of Nascent Vortex. This work can then be extended to unsteady cases.

2. Mathematical Model

In the present work, separated flow is assumed to be steady and is modelled by a single nascent vortex in the separated region as shown in Fig. 1, whose strength and the position along the chord are unknown.

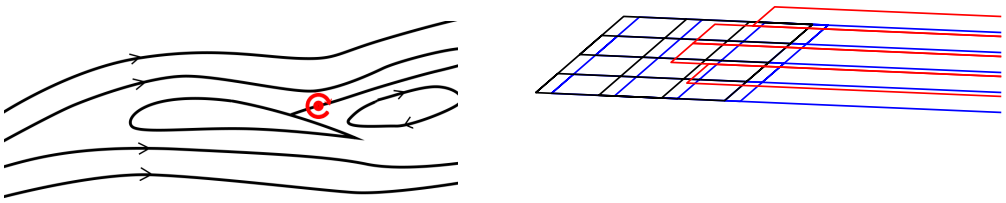

(a) Separated Flow in an airfoil (b) Separated Flow model for a 3D wing

Figure 1: Separated Flow

The airfoil characteristics in the inviscid regime are predicted by a discrete vortex element method (DVEM) as in Katz et al [8]. The inviscid model is extended to account for post-stall flow using a single nascent vortex with a fixed finite core as shown in Fig 1a in addition to DVEM.

The idea is that when viscous flow deviates from the inviscid flow $C_l - \alpha$ curve due to flow separation from the lifting surface, it essentially causes a deficit in the lift-creating vorticity around the airfoil. Therefore, if we can compensate for this loss in

vorticity, we should be able to get back the missing lift. The present method proposes to account for this missing vorticity by a nascent vortex of strength Γ_{nv} and position, x_{nv} along chord and z_{nv} perpendicular to the airfoil chord such that its effect on the airfoil is able to recover the loss in the coefficients of lift and pitching moment.

However, we have three unknowns (Γ_{nv}, x_{nv}, z_{nv}) and only two pieces of information ($\Delta C_l, \Delta C_m$) to evaluate these unknowns. Hence, one of the values must be assumed or found empirically so that a unique solution is obtained. In the present method, z_{nv} is assumed. Therefore, the effect of the nascent vortex (Γ_{nv}, x_{nv}) is expected to be such that it accounts for the residuals: $(C_l)_{visc} - (C_l)_{pot}$ and $(C_m)_{visc} - (C_m)_{pot}$. The unknowns are then solved iteratively so that they satisfy Eqn. 1.

$$J \cdot \delta x = -F \tag{1}$$

where

$$F = \begin{pmatrix} (C_l)_{pot} - (C_l)_{visc} \\ (C_m)_{pot} - (C_m)_{visc} \end{pmatrix} = \begin{pmatrix} \Delta C_l \\ \Delta C_m \end{pmatrix}$$

$$J = \begin{pmatrix} \frac{\delta \Delta C_l}{\delta \Gamma_{nv}} & \frac{\delta \Delta C_l}{\delta x_{nv}} \\ \\ \frac{\delta \Delta C_m}{\delta \Gamma_{nv}} & \frac{\delta \Delta C_m}{\delta x_{nv}} \end{pmatrix}; \qquad \delta x = \begin{pmatrix} \Delta \Gamma_{nv} \\ \Delta x_{nv} \end{pmatrix}$$

The $C_l - \alpha$ and $C_m - \alpha$ from the present methodology are plotted along with the input experimental data from Abbott [10] in Fig. 2.

The core radius (cr) of the Nascent Vortex is an important parameter. The effect of variation of the size of the core on the strength and position of the NV for NACA0009 is shown in Fig. 3. It is found that for $cr = 0.025$ and $cr = 0.05$, convergence does not occur for some α, while for some α the nascent vortex is located beyond the trailing edge, which is physically not possible.

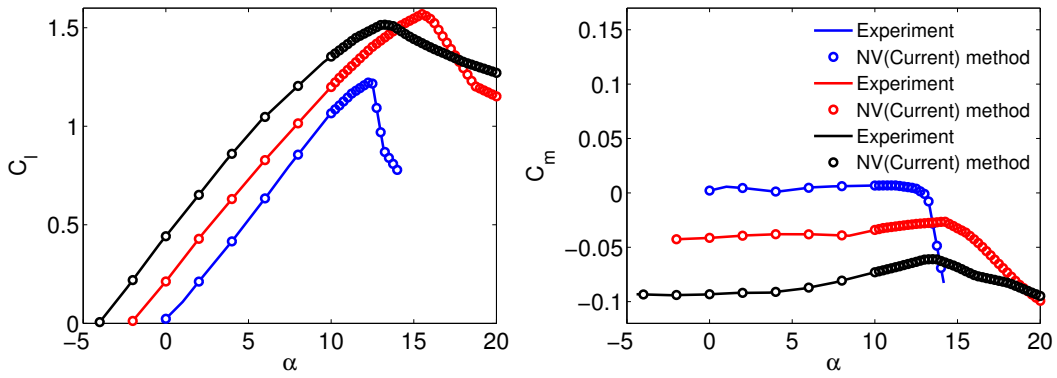

Figure 2: Aerodynamic Characteristics. Blue: NACA0009, Red: NACA2412, Black: NACA4412.

With increase in cr, the NV moves closer to the leading edge and the predicted circulation also increases. This trend is similar to the one observed when the z_{nv} is increased. Hence, a core radius of at least 0.1 has to be used. For all of the current calculations, a $cr = 0.2$ is used.

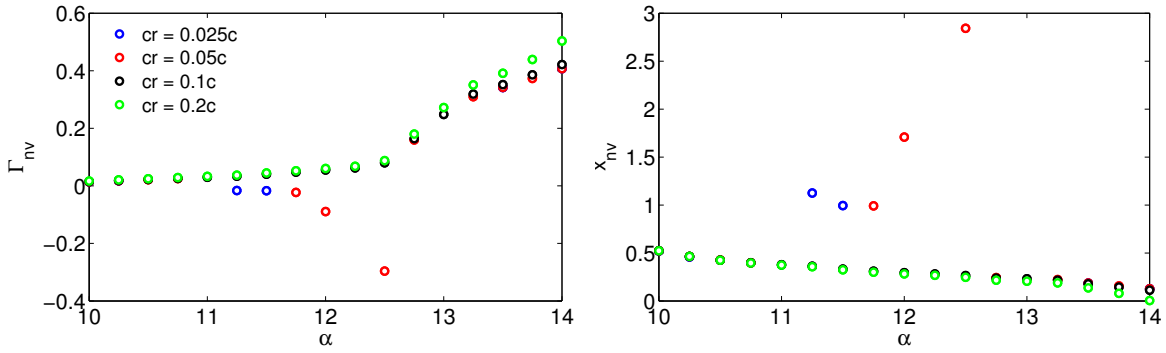

Figure 3: Variation of Γ_{nv} & x_{nv} with core radius (cr)

2.1. Implementation of Methodology for a 3D Wing

The inviscid solution of a 3D wing is obtained by using a Steady Vortex Lattice Method(VLM) [8]. The nascent vortex concept illustrated for a 2D airfoil is incorporated into the solution for a 3D wing, where the separated flow is modelled by horse-shoe vortices as shown in Fig. 1b. For the 3D solution, Eqn. 1 transforms to Eqn. 2.

$$J_{(2NY\times 2NY)} \cdot \delta x_{(2NY\times 1)} = -F_{(2NY\times 1)} \tag{2}$$

The local effective angle of attack $(\alpha_{eff})_i$ is computed using Eqn. 3.

$$(\alpha_{eff})_i = -sin^{-1}\left(\frac{K+G_i}{NX\times\left|\overrightarrow{U}_\infty\right|}\right); \qquad i=1,NY \tag{3}$$

Where,

$$K_i = \sum_{k=1}^{NX}\sum_{l=1}^{NX}\left(\left(\overrightarrow{V_b}\right)_{lk}\cdot\hat{n_k}\right)_i; \qquad G_i = \sum_{k=1}^{NX}\left(\left(\overrightarrow{V}_{nv}\right)_{ik}\cdot\hat{n_k}\right)_i;$$

$\left(\overrightarrow{V_b}\right)_{lk}$ is the velocity induced by the bound vortex of panel l on the collocation point of panel k; $\left(\overrightarrow{V}_{nv}\right)_{ik}$ is the velocity induced by the Nascent Vortex on section i on collocation point of panel k; $\hat{n_k}$ is unit normal vector to panel k and $\overrightarrow{U}_\infty$ is the free stream velocity.

Solve Eqn. 2 for the entire wing and find $\Delta\Gamma_{nv_i}$ & Δx_{nv_i}

$$\begin{pmatrix} \frac{\delta\Delta C_{l_j}}{\delta\Gamma_{nv_i}} & \frac{\delta\Delta C_{l_j}}{\delta x_{nv_i}} \\ \frac{\delta\Delta C_{m_j}}{\delta\Gamma_{nv_i}} & \frac{\delta\Delta C_{m_j}}{\delta x_{nv_i}} \end{pmatrix}\begin{pmatrix} \Delta\Gamma_{nv_i} \\ \Delta x_{nv_i} \end{pmatrix} = -\begin{pmatrix} \Delta C_{li} \\ \Delta C_{mi} \end{pmatrix}$$

Where $i=1,NY$; $j=1,NX$

3. Results

The present work is compared with the experimental work of Naik and Ostowari [11] for a rectangular wing of aspect ratio 12 at $Re = 0.5\times10^6$ & 0.75×10^6 as shown in

Fig. 4. Airfoil data is required as input, which is also available from the above reference. NACA4415 airfoil is used. No thickness correction is applied. $NY = 16$ is used.

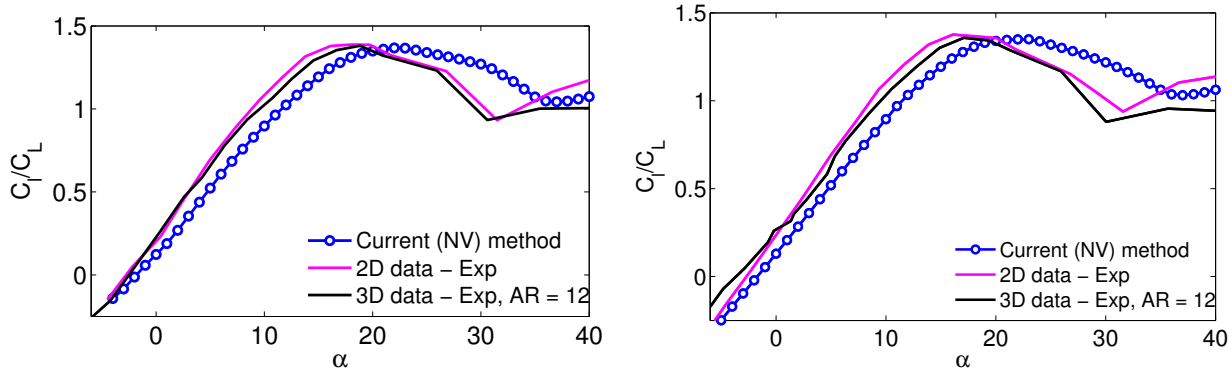

(a) Re $= 0.5 \times 10^6$ (b) Re $= 0.75 \times 10^6$

Figure 4: $C_L - \alpha$ for a finite wing (section: NACA 4415, $AR = 12$).

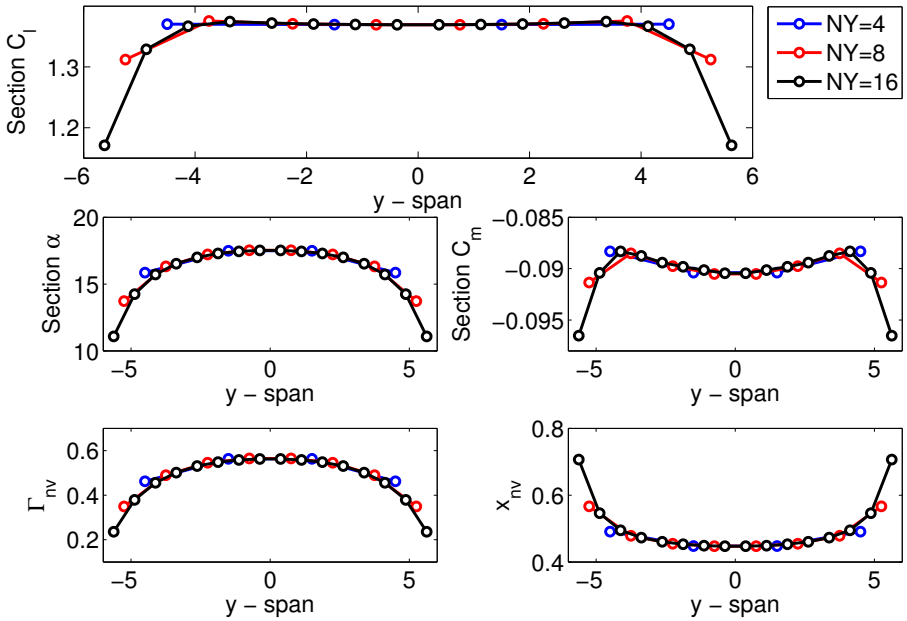

Figure 5: Variation along span of rectangular wing (section: NACA 4415, $AR = 12$, α=20^o).

It is seen from the 2D and 3D experimental plots in Fig. 4 that the airfoil and wing stall at $\alpha \approx 18^o$, which corresponds to a maximum $C_l \approx 1.4$ while the present results show that the wing is near-stall at $\alpha \approx 20^o$ for a similar maximum C_l. It is seen in Fig. 5 that in the root section of the wing, section $\alpha \approx 18^o$, which corresponds to a maximum $C_l \approx 1.4$. This is confirmed by the section C_l distribution. The high section C_l causes very high induced velocities near the root-section and hence there is an increase in the negative C_m. Conversely, the sectional distribution of the strength and location along

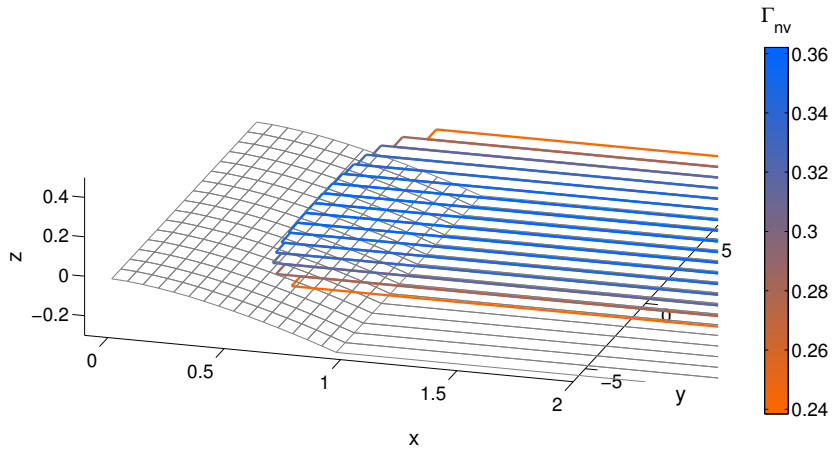

Figure 6: Distribution of circulation over Rectangular Wing(section: NACA 4415, $AR = 12$, α=15^o)

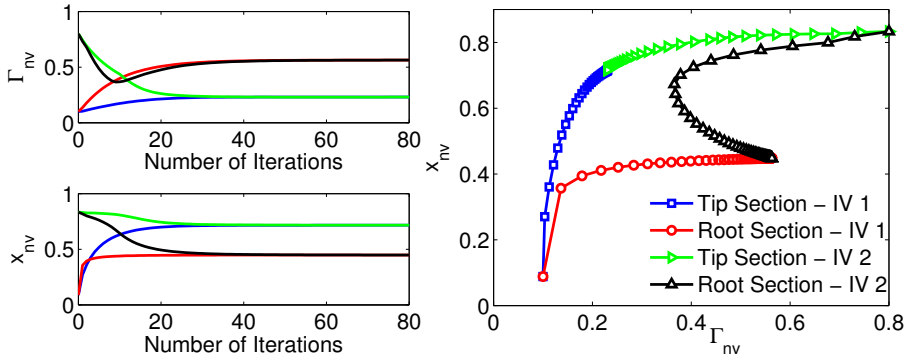

Figure 7: Effect of number of iterations and initial conditions on rectangular wing (section: NACA 4415).

chord of the nascent vortex show that Γ_{nv} is stronger and x_{nv} is nearly 0 near the root, suggesting that the vortex moves closer to the leading edge. It is interesting to note that even at the wing tips, Γ_{nv} is not close to zero. A particular case of the distribution of Γ_{nv} along the wing span at $\alpha = 15^o$ is shown in Fig. 6, where it clearly shows that the strength of the nascent vortex is stronger near the root and weakest near the tips for a rectangular wing.

The section C_l distribution is clearly devoid of any sawtooth and this result is obtained without the use of any *smoothing algorithm*. This is definitely a clear advantage over the post-stall predictive tool developed by Mukherjee et. al. [1].

The variation in Γ_{nv} & x_{nv} at the root and tip sections as the iterations progress is shown in Fig. 7 for a wing with NACA 4415 section, $\alpha = 20^o$, $AR = 12$ & $NY = 16$. Effect of initial conditions on Γ_{nv} & x_{nv} is studied at the tip and root sections for two different initial values for a final converged result. The initial values used are as follows: IV 1: Γ_{nv}=0.1 & x_{nv}=0.1 and IV 2: Γ_{nv}=0.8 & x_{nv}=0.8. For initial values of Γ_{nv}=0.9

& $x_{nv} = 0.9$ the solution did not converge. Hence, different initial values did not result in multiple solutions for a post-stall angle of attack.

4. Conclusion

A multi-dimensional post-stall predictive tool is developed for wing(s) using VLM, which uses a nascent vortex to account for flow separation. The tool is robust for wings with cambered airfoil sections but some convergence issues exist for wings with symmetric airfoil sections. For wings with cambered airfoil sections, section C_l distributions are completely devoid of sawtooth. Different initial conditions do not result in multiple solutions.

References

[1] Mukherjee, R., and Gopalarathnam, A., *Post-Stall Prediction of Multiple-Lifting-Surface Configurations Using a Decambering Approach*, Journal of Aircraft, Vol. 43, No. 3, pp. 660-668, May-June 2006.

[2] Sarpkaya T., *Computational Methods With Vortices-The 1988 Freeman Scholar Lecture*. ASME. J. Fluids Eng., 111(1):5-52, 1989. doi:10.1115/1.3243601.

[3] Katz J., *Large-scale vortex-lattice model for the locally separated flow overwings*. AIAA Journal 20:12, 1640-1646, 1982.

[4] Enrico G. A. Antonini, Gabriele Bedon, Stefano De Betta, Luca Michelini, Marco Raciti Castelli, and Ernesto Benini, *Innovative Discrete-Vortex Model for Dynamic Stall Simulations*. AIAA Journal 2015 53:2, 479-485.

[5] Sarpkaya T., *An inviscid model of two-dimensional vortex shedding for transient and asymptotically steady separated flow over an inclined plate*. Journal of Fluid Mechanics, 68, pp 109-128, 1975.

[6] Alexandre Joel Chorin. *Numerical study of slightly viscous flow*. Journal of Fluid Mechanics, 57, pp 785-796, 1973.

[7] A Leonard, *Vortex methods for flow simulation*. Journal of Computational Physics, Volume 37, Issue 3, Pages 289-335, ISSN 0021-9991, October, 1980.

[8] Katz, Joseph and Allen Plotkin. *Low-Speed Aerodynamics*. 2nd ed. Cambridge: Cambridge University Press, 2001.

[9] Leishman, J. G. *Principles of helicopter aerodynamics*. Cambridge: Cambridge University Press, 2006.

[10] Ira H. Abbott, Albert E. von Doenhoff, Louis S. Stivers, *Summary of airfoil data*. NACA Report, No. 824, 1945.

[11] Ostowari, C. and Naik, D., *Post Stall Studies of Untwisted Varying Aspect Ratio Blades with an NACA 4415 Airfoil Section Part 1*, Wind Engineering, Vol. 8, No. 3, 1984,pp. 176194.